

# Sensitivity of isolated photon production at TeV hadron colliders to the gluon distribution in the proton

Raphaëlle Ichou<sup>1</sup> and David d’Enterria<sup>2</sup>

<sup>1</sup>*SUBATECH, 4 rue Alfred Kastler, BP 20722, 44307 Nantes Cedex 3, France*

<sup>2</sup>*ICREA & ICC-UB, Universitat de Barcelona, 08028 Barcelona, Catalonia*

We compare the single inclusive spectra of isolated photons measured at high transverse energy in proton-antiproton collisions at  $\sqrt{s} = 1.96$  TeV with next-to-leading order perturbative QCD predictions with various parametrizations of the parton distribution functions (PDFs). Within the experimental and theoretical uncertainties, the Tevatron data can be reproduced equally well by the recent CTEQ6.6, MSTW08 and NNPDF1.2 PDF sets. We present also the predictions for isolated  $\gamma$  spectra in proton-proton collisions at  $\sqrt{s} = 14$  TeV for central ( $y = 0$ ) and forward ( $y = 4$ ) rapidities relevant for LHC experiments. Different proton PDFs result in maximum variations of order  $\pm 30\%$  in the expected  $E_T$ -differential isolated  $\gamma$  cross sections. The inclusion of the isolated photon data in global PDF fits will place extra independent constraints on the gluon density.

PACS numbers: 13.85.Ni 12.38.-t 12.38.Bx 13.87.Fh

## I. INTRODUCTION

The production of photons with large transverse energy ( $E_T \gg \Lambda_{\text{QCD}} \approx 0.2$  GeV) in high-energy hadronic collisions is an interesting process in itself as a testing ground of the perturbative regime of Quantum Chromodynamics (pQCD) [1], as well as a possible background for important new physics searches (such as e.g. often exemplified in the Higgs boson decay into two high- $E_T$  photons [2]). From a pQCD perspective, prompt photons issuing from hard parton-parton scatterings constitute a particularly clean testbed of perturbation theory in the collinear- [3, 4] and  $k_T$ - [5] factorization (or colour-dipole [6, 7]) approaches as well as of various logarithmic resummation techniques [8]. In addition, high- $E_T$  photons also yield valuable information about non-perturbative objects such as the parton distribution functions (PDFs) in the proton [9, 10] and the parton-to-photon fragmentation functions (FFs) [11, 12]. At lowest order in the electromagnetic and strong coupling constants  $\mathcal{O}(\alpha \alpha_s)$ , three partonic mechanisms produce prompt photons in hadronic collisions: (i) quark-gluon Compton scattering  $qg \rightarrow \gamma q$ , (ii) quark-antiquark annihilation  $q\bar{q} \rightarrow \gamma g$ , and (iii) the collinear fragmentation of a final-state parton into a photon<sup>1</sup>, e.g.  $qq \rightarrow qq \rightarrow \gamma X$ . The photons produced in the two first point-like processes are called “direct”, the latter “fragmentation” photons. The Compton channel is particularly interesting as it provides direct information on the proton gluon distribution,  $g(x, Q^2)$ , which is otherwise only *indirectly* constrained via the derivative of the proton structure function  $\partial F_2(x, Q^2)/\partial \log Q^2$  (“scaling violations”) in deep-inelastic scattering (DIS)  $e$ - $p$  collisions [14].

Experimentally – see e.g. [15, 16] for data compilations – many measurements of high- $E_T$  photon production have been carried out in the last 30 years in proton-proton ( $p$ - $p$ ) and proton-antiproton ( $p$ - $\bar{p}$ ) collisions at fixed-target and collider energies spanning center-of-mass (c.m.) energies of  $\sqrt{s} \approx 20 - 2000$  GeV. Apart from results at fixed-target energies from the E706 experiment [19], the agreement between data and theory is very good over nine orders of magnitude in the cross sections [16]. In order to identify the prompt photon signal out of the overwhelming background of photons from the decays of  $\pi^0$  and  $\eta$  mesons produced in the fragmentation of jets, one often requires the photon candidates to be isolated from any hadronic activity within a given distance around its direction. The corresponding measurements are then dubbed “isolated photons”. The most recent<sup>2</sup>  $E_T$ -differential spectra for isolated  $\gamma$  – measured at RHIC ( $p$ - $p$  at  $\sqrt{s} = 200$  GeV) [17] and Tevatron ( $p$ - $\bar{p}$  at  $\sqrt{s} = 1.96$  TeV) [18, 20] – can be well reproduced by theoretical predictions based on Next-to-Leading Order (NLO) pQCD calculations.

<sup>1</sup> Though at first sight such a process is  $\mathcal{O}(\alpha \alpha_s^2)$ , the fragmentation function of the outgoing parton into a photon scales as  $\alpha/\alpha_s$  and the corresponding cross section is of the same order as the direct process [13].

<sup>2</sup> Not included in the aforementioned data compilations.

Despite the existence of a few hundred data points, the inclusive and isolated photon data measured in  $p$ - $p$  and  $p$ - $\bar{p}$  collisions have not been considered in the last ten years in the global-fit analyses performed to determine the proton PDFs. The last PDF parametrization to use the photon data was MRST99 [21]. The theoretical difficulties to reproduce the fixed-target E706 results at  $\sqrt{s} \approx 30$  GeV [19] motivated their removal from the PDF studies. Instead, Tevatron jet data were preferred over photon data in global analysis to constrain the (high- $x$ ) gluon PDF. The available comparisons of the latest measured isolated photon spectra to NLO have been carried out with just one or two PDF parametrizations, e.g. CTEQ6.1M [22] and MRST04 [23], obtained a few years ago. Recently, new PDF sets have become available<sup>3</sup>—CTEQ6.6 [24], MSTW08 [25] and NNPDF1.2 [26]—which include the most up-to-date fits to data from deep-inelastic lepton-proton scattering and hadronic collisions as well as various theoretical improvements. The purpose of this paper is twofold. Firstly, we want to compare the existing Tevatron data to the theoretical predictions obtained using these latest PDF sets. Secondly, we want to study the expected sensitivity of near-future isolated photon spectra at the LHC to the same three sets of PDF parametrizations.

The paper is organized as follows. In Section II we succinctly remind the theoretical framework of our study and present the next-to-leading-order pQCD Monte Carlo (MC) programme JETPHOX that we have used. In Section III, we present a comparison of the existing Tevatron isolated photon spectra with the JETPHOX results for various PDFs, theoretical scales and FFs. We then present in Section IV the predictions for LHC energies, at central rapidities ( $y = 0$ ) accessible to the ALICE [28], ATLAS [29] and CMS [30] experiments as well as at the forward rapidities (up to  $y = 5$ ) covered by LHCb [31]. We discuss the associated uncertainties in the spectra and the sensitivity to the underlying PDFs. We summarize our main findings in Section V.

## II. THEORETICAL FRAMEWORK

### A. Inclusive prompt photon production

As aforementioned, two types of processes contribute to the prompt photon production cross section in  $p$ - $p$  and  $p$ - $\bar{p}$  collisions: the ‘direct’ contribution, where the photon is emitted directly from a pointlike coupling to the hard parton-parton vertex, and the ‘fragmentation’ (sometimes also called ‘anomalous’) contribution, in which the photon originates from the collinear fragmentation of a final-state parton. Schematically, the differential photon cross section in transverse energy  $E_T$  and rapidity  $y$  can be written as [16]:

$$d\sigma \equiv d\sigma_{dir} + d\sigma_{frag} = \sum_{a,b=q,\bar{q},g} \int dx_a dx_b F_a(x_a; \mu_F^2) F_b(x_b; \mu_F^2) \times \quad (1)$$

$$\left[ d\hat{\sigma}_{ab}^\gamma(p_\gamma, x_a, x_b; \mu_R, \mu_F, \mu_{ff}) + \sum_{c=q,\bar{q},g} \int_{z_{min}}^1 \frac{dz}{z^2} d\hat{\sigma}_{ab}^c(p_\gamma, x_a, x_b, z; \mu_R, \mu_F, \mu_{ff}) D_c^\gamma(z; \mu_{ff}^2) \right]$$

where  $F_a(x_a, \mu_F)$  is the parton distribution function of parton species  $a$  inside the incoming hadrons  $h$  at momentum fraction  $x_a$ ;  $D_{\gamma/k}(z, \mu_{ff})$  is the fragmentation function of parton  $k$  to a photon carrying a fraction  $z$  of the parent parton energy (integrated from  $z_{min} = x_T \cosh y$ , with  $x_T = 2E_T/\sqrt{s}$ , to 1); and the arbitrary parameters  $\mu_R$ ,  $\mu_F$  and  $\mu_{ff}$  are respectively the renormalisation, initial-state factorisation, and fragmentation scales which, loosely speaking, encode any residual dependence of the cross sections to higher-order contributions missing in the calculation. The study provided in this article relies on the calculation of both  $d\sigma_{dir}$  and  $d\sigma_{frag}$  at next-to-leading order (NLO) accuracy [32] in the strong coupling  $\alpha_s(\mu_R)$ , i.e. all diagrams up to the order  $\mathcal{O}(\alpha_s^2)$  are included, defined in the  $\overline{\text{MS}}$  renormalisation scheme.

---

<sup>3</sup> During the completion of this work, the NNPDF collaboration released new PDF sets (NNPDF2.0) [27]. Although the gluon PDF has changed, it is consistent with the NNPDF1.2 version used here, and we do not expect significant differences on the photon production predictions.

The results of the NLO calculation of  $d\sigma_{dir}$  have been known for a long time [3]. The calculation of the NLO corrections to  $d\sigma_{frag}$  became also available later [4, 13, 32]. We note that the distinction between  $d\sigma_{dir}$  and  $d\sigma_{frag}$  is arbitrary (only its sum is physically observable): a typical case is a bremsstrahlung process from a final-state quark which, depending on the scale, can be considered as “fragmentation” or as “NLO direct”.

More recently, expressions involving the resummation – at next-to-leading (NLL) or even next-to-next-to-leading (NNLL) logarithmic accuracy – of threshold and recoil contributions due to soft gluon emission, which are large close to the phase space boundary where the  $E_T$  of the photon is about half of the center-of-mass energy ( $x_T = 2E_T/\sqrt{s} \rightarrow 1$ ) have been obtained for  $d\sigma_{dir}$  and  $d\sigma_{frag}$  [8]. The effect of this resummation is important at very large<sup>4</sup> photon  $E_T$  extending down to values of  $x_T \approx 10^{-1}$ , and provide a much reduced  $\mu_R$  and  $\mu_F$  scale dependence than the NLO approximation. In any case, since we are interested in the low- $x$  region of the PDFs, we do not consider such effects, which are not implemented in JETPHOX, in this study.

In Figure 1 we show the kinematical region covered by the photon measurements in the  $(x_T, E_T^2)$  plane equivalent to the DIS  $(x, Q^2)$  plane for hard scattering hadronic processes. The quoted  $x$  values are typical  $x_T$  values for measurements at midrapidity and  $x \approx x_T \cdot \exp(-y)$  at forward rapidities. At midrapidities, photon production at the LHC will probe values 20 times smaller than at Tevatron because of the factor  $\sim 7$  increase in the c.m. energy and the lower  $E_T$  values reachable (e.g. down to  $E_T \approx 5$  GeV at ALICE). At the forward rapidities and low  $E_T \approx 5$  GeV covered e.g. by LHCb, one can probe the gluon distribution down to very small  $x \approx 10^{-5}$ . The combined photon data at all energies – about 350 data-points collected so far plus  $\mathcal{O}(100)$  new data-points expected from the four experiments at the LHC – provide thus constraints of the PDFs in a wide  $(x, Q^2)$  range.

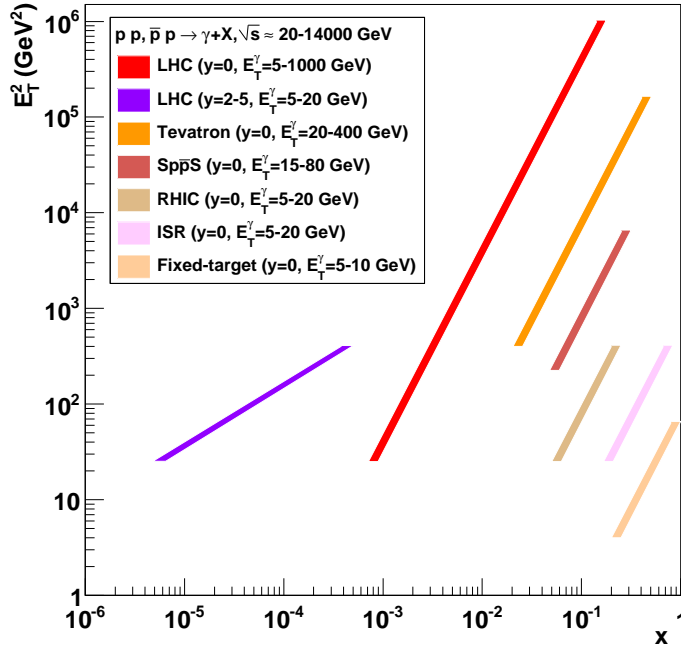


FIG. 1: Kinematical region probed by existing prompt photon measurements at fixed-target (Fermilab) and collider (ISR, RHIC, SpS, Tevatron) energies, and expected range probed at the LHC at central ( $y = 0$ ) and forward ( $y = 2 - 5$ ) rapidities.

In Figure 2 we show the relative contributions of each one of the three subprocesses (Compton,

<sup>4</sup> Note that at the highest momenta probed, there are also additional corrections due to electroweak boson exchanges, which decrease the photon yields by about 10–20% within  $E_T^\gamma \approx 1 - 2$  TeV at the LHC [33].

annihilation and fragmentation) to prompt photon production at Tevatron ( $y = 0$ ) and LHC ( $y = 0$ , and  $y = 4$ ) as a function of the photon  $E_T$ . [Again, the plots are to be taken indicatively as the weights of the different components are scale-dependent.] They have been obtained selecting the corresponding Feynman diagrams at NLO with the JETPHOX MC, setting all scales to  $\mu = E_T^\gamma$ , and using the CTEQ6.6 parton densities and the BFG-II parton-to-photon FFs for the fragmentation photons. In the low  $E_T$  region of the mid-rapidity spectra (below 15 GeV at Tevatron, and 40 GeV at the LHC) the fragmentation component dominates the cross sections. At the Fermilab collider, quark-gluon scattering is the dominant component up to  $E_T \approx 120$  GeV, beyond which the annihilation of valence (anti)quarks from the (anti)proton beams play a preeminent role. At the LHC, the Compton process dominates for all  $E_T$ 's above 45 GeV at  $y = 0$ . At forward rapidities at the LHC, between 50% to 80% of inclusive prompt photons are produced from the collinear fragmentation of a parton for all relevant  $E_T$ 's.

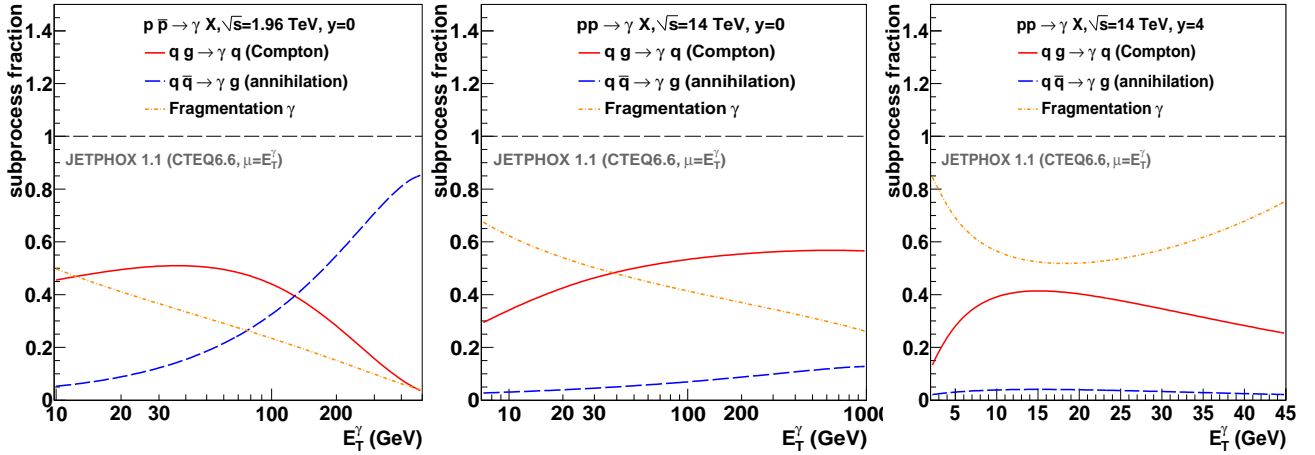


FIG. 2: Relative contributions of the quark-gluon Compton,  $q\bar{q}$  annihilation and fragmentation subprocesses in NLO prompt photon production at the Tevatron (left), LHC midrapidity (center) and LHC forward rapidity (right) obtained with JETPHOX (CTEQ6.6 PDF,  $\mu = E_T^\gamma$ , and BFG-II FFs).

## B. Isolated photon production

In order to strongly suppress the overwhelming background of secondary photons coming from the electromagnetic hadron decays (mainly  $\pi^0$  and  $\eta$  mesons) produced inside partonic jets, collider experiments require often an isolation criterion on the photon candidates. A standard isolation requirement is that within a cone about the direction of the photon defined in rapidity  $y$  and azimuthal angle  $\phi$  by

$$R = \sqrt{(y - y_\gamma)^2 + (\phi - \phi_\gamma)^2}, \quad (2)$$

the accompanying hadronic transverse energy  $E_T^{had}$  is less than a given value

$$E_T^{had} \leq E_T^{max}. \quad (3)$$

$R$  is usually taken between 0.4 – 0.7 and  $E_T^{max}$  is specified either as a fixed value, or as a fixed fraction  $\varepsilon_h$  (e.g. often 10%) of the photon  $E_T$ . Cross sections for producing isolated photons have been proven to fulfill the factorization theorem, and are finite to all orders in perturbation theory for non zero  $R$  and  $E_T^{max}$  [34].

If one ignores the “underlying event” activity in the collision – due to soft interactions of spectator partons and beam remnants [35] – the leading-order  $qg$ -Compton and  $q\bar{q}$ -annihilation photons are emitted in a region completely free from hadronic activity (the recoiling quark or gluon is emitted at  $\pi$  from it).

On the other hand, the fragmentation component is usually accompanied by other particles issuing from the hadronization of the same parent parton (jet). Yet, the isolated cross section measured experimentally cannot be automatically identified with the direct cross section calculated at the Born level. First, higher order terms originating in the *non-collinear* fragmentation of partons also contribute to the isolated cross sections. Second and most important, although isolation cuts such as Eqs. (2), (3) reduce the  $d\sigma_{frag}$  contribution, a fraction of fragmentation photons with  $z \geq 1/(1 + \varepsilon_h)$  survive the cuts [16]. The average  $z$ -value for fragmentation photons is  $\langle z \rangle \lesssim 0.6$  at the LHC and  $\langle z \rangle \approx 0.7$  at the Tevatron [13], and a typical isolation energy cut of  $\varepsilon_h = 0.1$ , corresponding to  $1/(1 + \varepsilon_h) > 0.9$ , suppresses about 60 – 80% of  $d\sigma_{frag}$  (this value is  $E_T^\gamma$ - and scale-dependent). We see this in more detail in Fig. 3 where we show the subprocesses contributions to the *isolated* photon cross section. At variance with Fig. 2 for the inclusive prompt- $\gamma$  case, we can see that a very significant part of the fragmentation component is suppressed after applying typical isolation cuts ( $R = 0.4$ ,  $\varepsilon_h = 0.1$ ). The Compton process now clearly dominates the photon yield below  $E_T^\gamma \approx 120$  GeV at Tevatron and accounts for about 3/4 of isolated  $\gamma$  production for all  $E_T^\gamma$ 's at the LHC. These results confirm the interesting potential of isolated photon hadroproduction to constrain the gluon density.

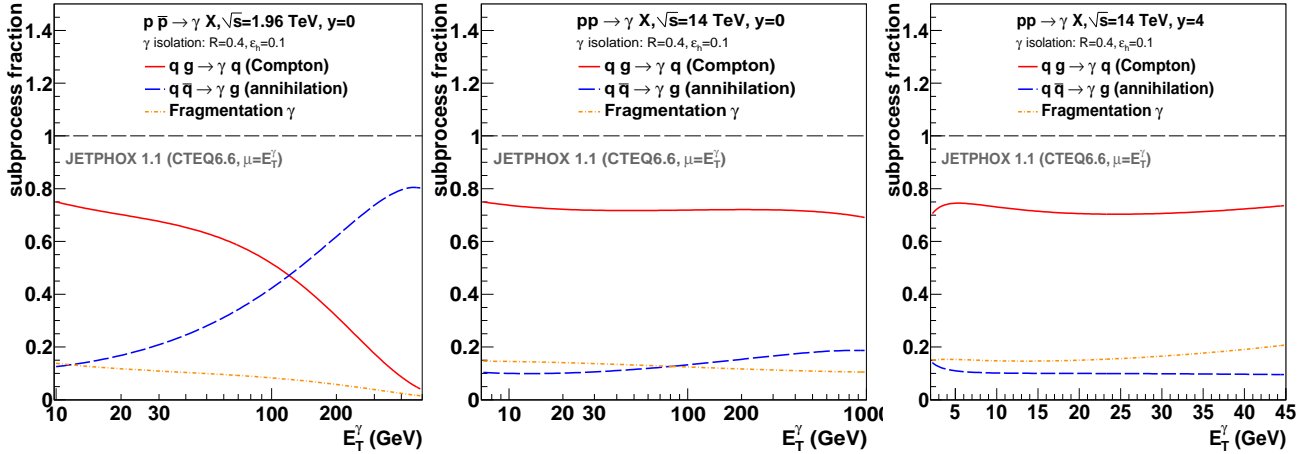


FIG. 3: Relative contributions of the quark-gluon Compton,  $q\bar{q}$  annihilation and fragmentation subprocesses in NLO *isolated* photon production at the Tevatron (left), LHC midrapidity (center) and LHC forward rapidity (right) obtained with JETPHOX (CTEQ6.6 PDF,  $\mu = E_T^\gamma$ , BFG-II FFs) for an isolation radius  $R = 0.4$  and a hadron fraction of the photon energy of  $\varepsilon_h = 0.1$  inside the cone.

### C. JETPHOX Monte Carlo

The present study relies on the implementation of the photon NLO calculation of both  $d\sigma_{dir}$  and  $d\sigma_{frag}$  in the JETPHOX Monte Carlo (MC) programme [32, 34]. The main advantage of the JETPHOX MC is that one can easily account for any kind of experimental cuts (e.g. on kinematics and/or isolation) implementable at the partonic level. In addition, one can match naturally the binning of experimental data by histogramming of the partonic configurations generated. All the NLO results provided in the following sections are obtained using<sup>5</sup>  $\alpha_s(M_Z) = 0.118$ , with up to 5 active quark flavours (the lowest  $E_T^\gamma$  considered in this work is close to  $m_b \approx 4$  GeV/ $c^2$ ). We switched off the box diagram  $gg \rightarrow g\gamma$  in the calculations because its contribution to the single inclusive spectrum is found to be of just a few percent. The CTEQ6.6, MSTW08 and NNPDF1.2 PDFs were interfaced to JETPHOX via the LHAPDF (version 5.7.1)

<sup>5</sup> Note that although each PDF set uses a slightly different reference value:  $\alpha_s(M_Z) = 0.118$  (CTEQ6.6),  $\alpha_s(M_Z) = 0.119$  (NNPDF1.2), and  $\alpha_s(M_Z) = 0.12018$  (MSTW08), the resulting differences in the  $\gamma$  cross sections obtained using the slightly different coupling choices are very small.

package [36]. Whenever the scales  $\mu_R$ ,  $\mu_F$  and  $\mu_{ff}$ , are given a common value, the latter is noted  $\mu$  hereafter.

In JETPHOX the NLO calculations are performed at the parton level and do not account for hadronisation effects which can be potentially large at low  $E_T$ . In addition, they do not include the soft hadronic activity from the underlying event (parton spectator collisions, beam remnants ...) whose transverse energy can also fall inside the isolation cone. However, the experimental data at Tevatron have been corrected for such effects. In the case of the CDF analysis, the correction is found to amount about 9% of the photon yield, independent of its  $E_T$  above 30 GeV [18]. Studies at the LHC using various tunes of the underlying event with PYTHIA [37] indicate that the loss of isolated photons due to hadronic activity within the isolation cone is of about 20% at  $E_T^\gamma \approx 5$  GeV and negligible above 70 GeV (for radius  $R = 0.4$  and hadronic energy fraction  $\varepsilon_h = 0.1$ ) [38].

### III. COMPARISON OF TEVATRON DATA TO NLO PQCD

During the Tevatron Run-II, the DØ and CDF collaborations collected respectively  $0.32 \text{ fb}^{-1}$  and  $2.5 \text{ fb}^{-1}$  worth of photon data in  $p\bar{p}$  collisions at  $\sqrt{s} = 1.96$  GeV [18, 20]. Such data sample allowed both experiments to measure isolated prompt photons in the  $E_T$  range from roughly 20 GeV to about 400 GeV. The detailed conditions of the measurements are as follows

- DØ: Kinematics:  $E_T^\gamma = 20 - 300$  GeV,  $|y^\gamma| < 0.9$ . Isolation criterion:  $R = 0.4$ ,  $\varepsilon_h = E_T^{had}/E_T^\gamma < 0.1$ .
- CDF: Kinematics:  $E_T^\gamma = 30 - 400$  GeV,  $|y^\gamma| < 1.0$ . Isolation criterion:  $R = 0.4$ ,  $E_T^{had} < 2$  GeV.

We have used the kinematics and isolation cuts in JETPHOX corresponding to each measurement and calculated the resulting isolated photon spectrum with the same  $E_T$  binning as the experimental spectra. The calculations have been repeated for three PDF sets (CTEQ6.6M, MSTW08, NNPDF1.2), three scales ( $\mu=0.5E_T^\gamma$ ,  $E_T^\gamma$ ,  $2E_T^\gamma$ ) and two photon FFs (BFG-I and BFG-II) [11]. The results are presented and discussed in the next subsections.

#### A. Parton distribution functions dependence

The DØ and CDF isolated photon spectra are compared in Fig. 4 to the corresponding JETPHOX predictions for three different PDF parametrizations (CTEQ6.6, MSTW08 and NNPDF1.2). The theoretical scales have been set to  $\mu = E_T^\gamma$  and the parton-to-photon FFs to the BFG-II set. The three theoretical spectra are very similar and they all agree well with the data within the experimental uncertainties given by the error bars (resp. bands) representing the statistical (resp. systematical) errors. The isolated photon spectrum obtained using MSTW08, for both sets of experimental cuts, is mostly in between the spectra obtained with the two other PDFs, except at small- $E_T^\gamma$  where MSTW08 results in a somewhat lower cross section, closer to the data. This is better seen in Fig. 5 where we plot the ratio data/theory calculated with the three choices of PDF. On average, the NNPDF1.2 (resp. CTEQ6.6) prediction is a few percents higher (resp. lower) than the MSTW08 distribution. As aforementioned, all PDFs reproduce well in magnitude and shape the experimental spectrum within the experimental uncertainties, dominated by the energy-scale uncertainty (orange bands in the plots).

A simple  $\chi^2$  analysis of the full spectrum to the theoretical predictions, accounting for the experimental uncertainties (statistical and systematical added in quadrature) yields  $\chi^2/ndf$  below 1 for the three PDF predictions. For the default scale-choice shown,  $\mu = E_T^\gamma$ , MSTW08 reproduces a bit better both the CDF and DØ results. One has to note, however, that in the  $E_T^\gamma$  range below  $\sim 40$  GeV a shape difference is apparent, with all NLO curves systematically under-predicting the steepness of the cross section by up to around 40% in the lowest  $E_T^\gamma$  bin. The source of such a disagreement, which is about a  $2\sigma$  effect in the case of DØ, is unclear. Theoretically, the inclusion of small- $x$  resummation effects [39] does not help to improve the data-NLO agreement.

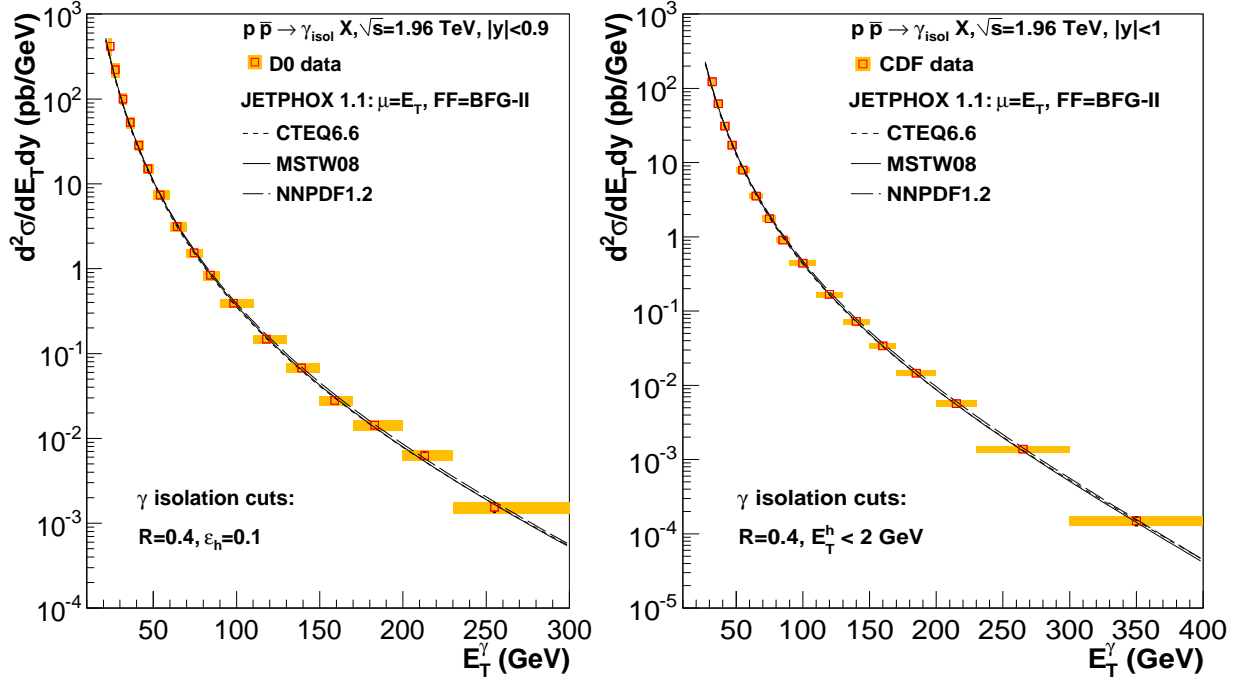


FIG. 4: Isolated photon  $E_T$ -differential cross section at mid-rapidity in  $p\bar{p}$  at  $\sqrt{s} = 1.96$  TeV measured by DØ (left) and CDF (right) compared to JETPHOX ( $\mu = E_T$ , BFG-II) for three different PDFs: CTEQ6.6, MSTW08 and NNPDF1.2. The (orange) bands indicate the experimental systematic errors.

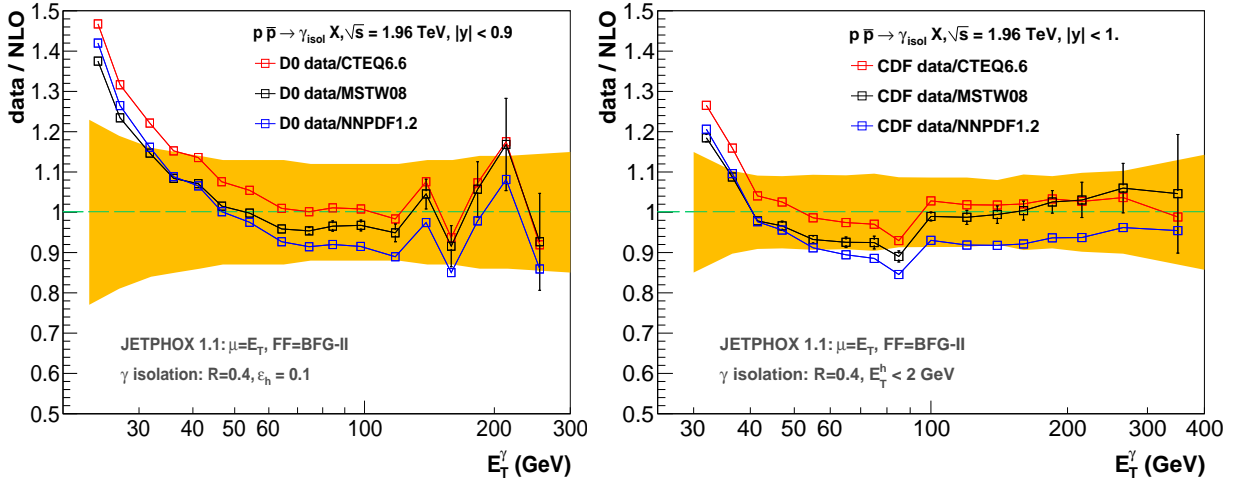


FIG. 5: Ratio of isolated photon midrapidity spectra in  $p\bar{p}$  at  $\sqrt{s} = 1.96$  TeV measured by DØ (left) and CDF (right) over the JETPHOX ( $\mu = E_T$ , BFG-II) predictions for three PDFs: CTEQ6.6, MSTW08 and NNPDF1.2. For clarity, only the MSTW08 ratio is shown with propagated statistical errors from the data. The lines between data/NLO points are to guide the eye. The (orange) bands indicate the systematic uncertainties of the measurements.

## B. Scale dependence

As mentioned in Section II A, the truncation of the  $\alpha_s$  expansion of the pQCD cross section for prompt photon production, Eq. (2), at a given order introduces an arbitrary dependence on three unphysical scales: the renormalization scale  $\mu_R$  which appears in the evolution of the coupling, the factorization scale  $\mu_F$  associated to collinear singularities in the PDFs, and the fragmentation scale  $\mu_{ff}$  related to collinear

singularities in the FFs. Since those scales are unphysical, the theory can be considered reliable only where the predictions are stable with respect to variations of them. Usually scale variations of a factor of two around the “natural” physical scale of the scattering process, often taken as the  $E_T$  of the photon, are considered:  $\mu = E_T^\gamma/2 - 2E_T^\gamma$ . In Fig. 6, we show the ratio of the JETPHOX isolated  $\gamma$  spectra at Tevatron obtained with scales set to  $\mu = E_T^\gamma/2$  and  $\mu = 2E_T^\gamma$  over the same spectrum for  $\mu = E_T^\gamma$ . In all three cases, we use the CTEQ6.6 PDFs<sup>6</sup> and the BFG-II FFs. The sensitivity to the changes in the theoretical scale  $\mu$  is of about  $\pm 10\%$  in the whole  $E_T$ -range. The choice of a scale value  $\mu = E_T^\gamma$  agrees better with the experimental spectrum for the MSTW08 and CTEQ6.6 PDFs whereas the NNPDF1.2, whose central spectrum is a bit higher than the two others, favours a larger  $\mu = 2E_T^\gamma$  scale.

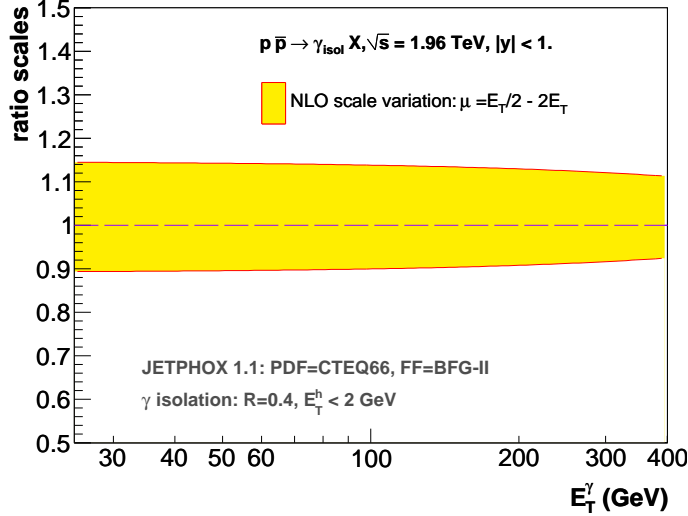


FIG. 6: Scale uncertainty of the JETPHOX NLO predictions for isolated photon production at Tevatron (CDF isolation cuts) plotted as the ratio of the spectrum obtained with  $\mu = 0.5E_T^\gamma, 2E_T^\gamma$  over that with  $\mu = E_T^\gamma$ .

### C. Dependence on the parton-to-photon fragmentation functions (FFs)

The production of fragmentation photons in hadronic collisions is completely encoded in the parton-to-photon FFs,  $D_{\gamma/k}(z, \mu_{ff})$  obtained from fits [11, 40] to photon production data at LEP ( $e^+e^- \rightarrow q\bar{q}(g) \rightarrow \gamma X$ ) [41]. In JETPHOX two choices of FFs are available: the BFG set I (“small gluon”) and II (“large gluon”) [11]. Although both FFs reproduce the LEP data, mostly sensitive to the high  $z = p_\gamma/p_{parton}$  range of the FFs, at small  $z$  the gluon-to-photon fragmentation function of set I is significantly lower than the one of set II. Otherwise, the quark-to-photon fragmentations are identical in BFG-I and BFG-II. We have run prompt and isolated photon production in the Tevatron kinematic range with JETPHOX at NLO with the two FF sets. The inclusive prompt  $\gamma$  spectrum obtained with BFG-I is just a few percent smaller than the one obtained with BFG-II, below  $E_T^\gamma \approx 80$  GeV. The corresponding BFG-I and BFG-II isolated photon spectra are virtually identical. This is not unexpected since a significant fraction, up to 80% (see Fig. 3), of the fragmentation photons are removed by standard isolation cuts  $R = 0.4$ ,  $\varepsilon_h = 0.1$ .

<sup>6</sup> The scale-dependence obtained with the two other PDF parametrizations are similar.



#### IV. ISOLATED PHOTON PRODUCTION AT THE LHC

At the top LHC center-of-mass energy of 14 TeV, the production cross section of isolated photons,  $\sigma(E_T^\gamma > 10 \text{ GeV})|_{y=0} = 300 \text{ nb}$  at NLO, is seven times higher than at Tevatron,  $\sigma(E_T^\gamma > 10 \text{ GeV})|_{y=0} = 40 \text{ nb}$ . This will allow one to carry out high-statistics measurements even with moderate integrated luminosities, without (or with minimal) pileup. The ALICE, ATLAS, CMS and LHCb experiments at the LHC have photon reconstruction capabilities with electromagnetic calorimetry in various rapidity ranges. The two general-purpose high-luminosity detectors ATLAS [29] and CMS [30] cover<sup>7</sup>  $|y| < 3$  from  $E_T \approx 10 \text{ GeV}$  up to very large  $E_T \approx 1 \text{ TeV}$ , whereas ALICE [28] covers  $|y| < 0.7$  in a range of moderate  $E_T \approx 5 - 100 \text{ GeV}$ . LHCb [31], on the other hand, can measure photons within  $2 < \eta < 5$  albeit up to relatively moderate  $E_T \approx 20 \text{ GeV}$ , as the calorimeter dynamic range is mostly optimised for low energy photons coming from  $B$ -mesons radiative decays. As possible benchmark measurements, we will consider isolated (radius  $R = 0.4$ ) photon production at  $y = 0$  (for ALICE, ATLAS and CMS) and at  $y = 4$  (for LHCb<sup>8</sup>). The JETPHOX predictions for central and forward rapidities for three different PDF parametrizations (CTEQ6.6, MSTW08 and NNPDF1.2) are shown in Fig. 7.

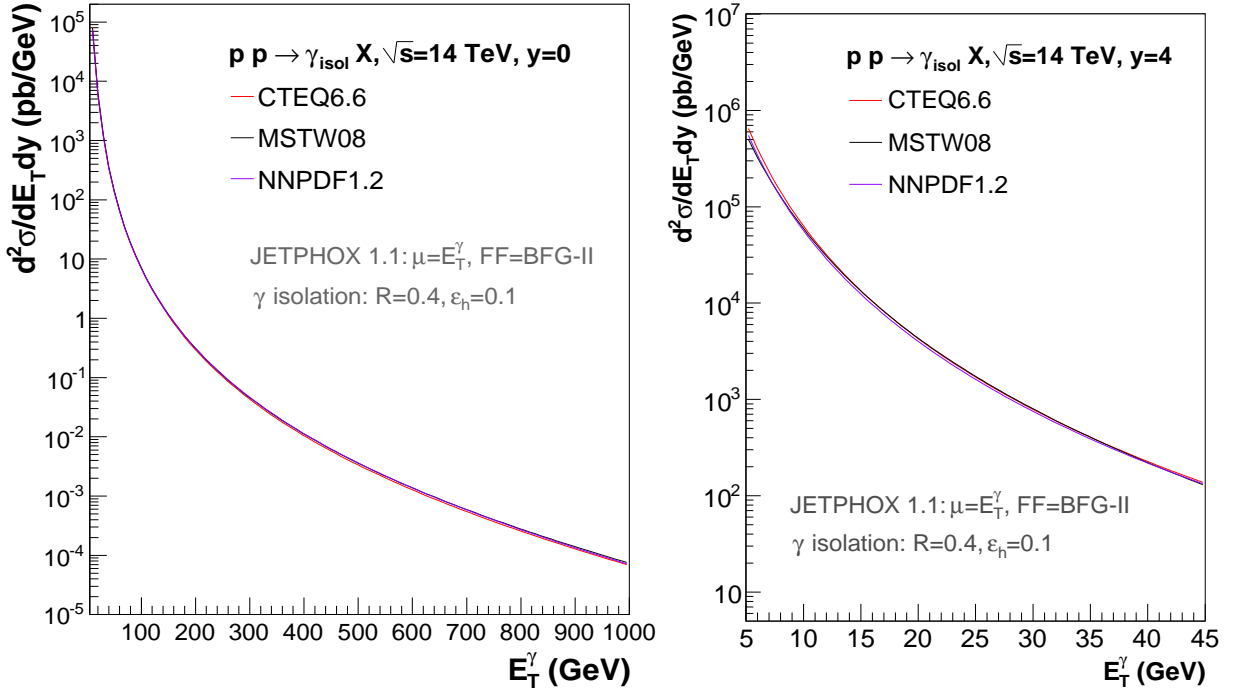


FIG. 7: Predictions of the isolated photon spectrum in  $p$ - $p$  collisions at  $\sqrt{s} = 14 \text{ TeV}$  obtained with JETPHOX (scales fixed at  $\mu = E_T^\gamma$  and FFs set to BFG-II) for three different PDF parametrisations (CTEQ6.6, MSTW08 and NNPDF1.2) for central ( $y = 0$ , left) and forward ( $y = 4$ , right) rapidities.

Differences of a few tens of percent in the photon spectra obtained with different PDFs are not noticeable in logarithmic plots such as those in Fig. 7. In Figure 8 we show the fractional differences,  $(1 \pm \text{PDF1}/\text{PDF2})$ , between the JETPHOX predictions for isolated photon spectra ( $R = 0.4$  and  $\varepsilon_h = 0.1$ ) obtained at  $y = 0$  in  $p$ - $p$  collisions at  $\sqrt{s} = 14 \text{ TeV}$  for the various PDF sets. They have been obtained with the CTEQ66, MSTW08 and NNPDF1.2 for fixed scales at  $\mu = E_T^\gamma$  and BFG-II FF. In general, the agreement among different PDFs is very good except at very low and very high  $E_T^\gamma$ . The choice

<sup>7</sup> We do not consider here the possibilities covered by the ATLAS and CMS forward hadron calorimeters up to  $|y| < 5$ .

<sup>8</sup> The chosen rapidity  $y = 4$ , lower than the maximum LHCb  $y = 5$  value, accounts for the effect of the  $R = 0.4$  isolation radius and possible additional fiducial cuts.

of PDF results in up to  $\sim 15\%$  variations of the photon yields below  $E_T^\gamma \approx 15$  GeV (left plot). Similar PDF uncertainties are obtained within one single PDF parametrization. As an example in the right plot we show the envelope of maximum relative differences at each  $E_T^\gamma$  between each one of the ten<sup>9</sup> first NNPDF1.2 replicas and the default (central) NNPDF1.2 set.

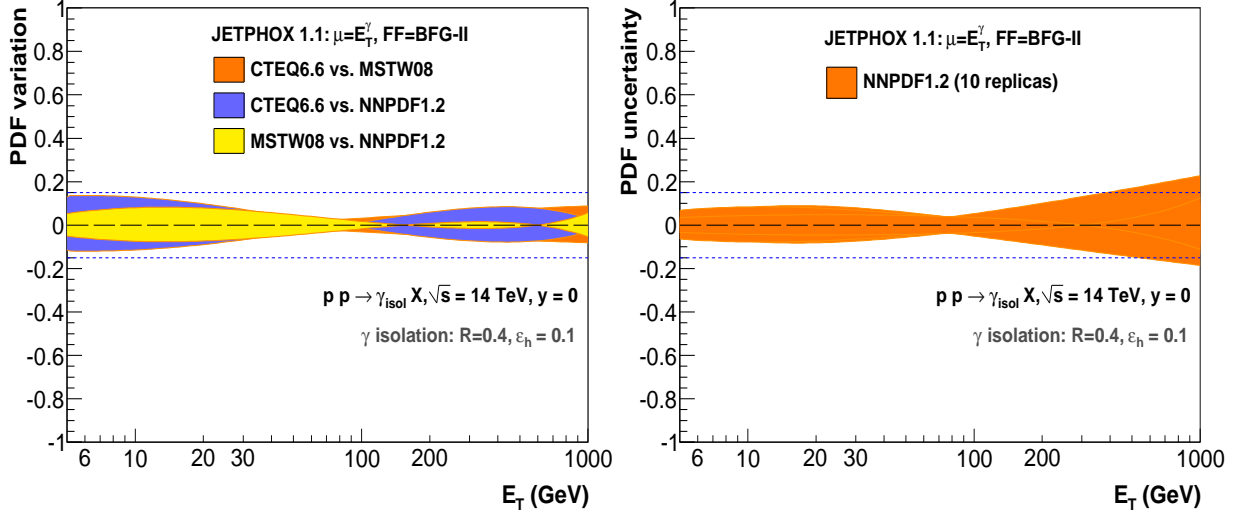


FIG. 8: Fractional differences between the isolated photon spectrum in  $p$ - $p$  collisions at  $\sqrt{s} = 14$  TeV at *central* rapidities ( $y = 0$ ) obtained with JETPHOX (scales fixed at  $\mu = E_T^\gamma$ , FF set to BFG-II) using: (a) three different PDF parametrizations (CTEQ6.6, MSTW08 and NNPDF1.2), and (b) ten NNPDF1.2 replicas over the reference parametrization of the same PDF set. The dashed lines indicate a  $\pm 15\%$  uncertainty.

The expected PDF sensitivity for measurements of *forward* isolated photons ( $y = 4$ ) in the transverse energy range  $E_T = 5 - 50$  GeV is shown in Figure 9. Variations in the photon yields of up to  $\sim 30\%$  depending on the PDF set can be seen at the lowest  $E_T^\gamma \approx 5$  GeV (left plot). Intra-PDF uncertainties seem to be somewhat lower (around  $\sim 15\%$  within 10 replicas of the NNPDF1.2 parametrization, right plot).

As in the Tevatron case, the dominant source of experimental uncertainty (orange bands in Fig. 4) in any (isolated or not) photon measurement at the LHC will likely come from the uncertainty in the absolute energy scale of the calorimeters. A typical 1.5% uncertainty in the photon energy calibration will propagate into about 10% uncertainties in the photon cross sections for a steeply-falling photon spectrum with inverse power-law exponent  $n \approx 5 - 8$ . Altogether, ten to fifteen percent uncertainties in the final cross sections (not accounting for an overall luminosity normalization error) are to be expected at the LHC. Those values are usually better than the uncertainties linked to jet measurements where the energy-scale uncertainty, involving a good knowledge of the hadronic calorimeters calibration, is often poorer than for photons.

In the theoretical side, as seen in the case of the Tevatron predictions (Section III), the choice of the parton-to-photon FF plays no role on the final isolated photon cross sections and we are left with the choice of theoretical scales  $\mu_R$ ,  $\mu_F$  and  $\mu_{ff}$  as the only important source of uncertainty. In Figure 10, we present the fractional differences,  $(1 \pm \mu'/\mu)$ , between the predicted isolated photon spectra obtained with JETPHOX (MSTW08 PDFs and BFG-II FFs) with “default” theoretical scale ( $\mu = E_T^\gamma$ ) and those obtained with  $\mu' = E_T^\gamma/2 - 2E_T^\gamma$ . At low  $E_T$  the uncertainty in the cross sections linked to scales variations amounts to up to  $\pm 20\%$  but it saturates at around  $\pm 10\%$  above  $E_T^\gamma \approx 15$  GeV at central and forward

<sup>9</sup> Although this is a relatively small number of replicas, running JETPHOX at NLO is a quite time-expensive operation from the computational point of view.

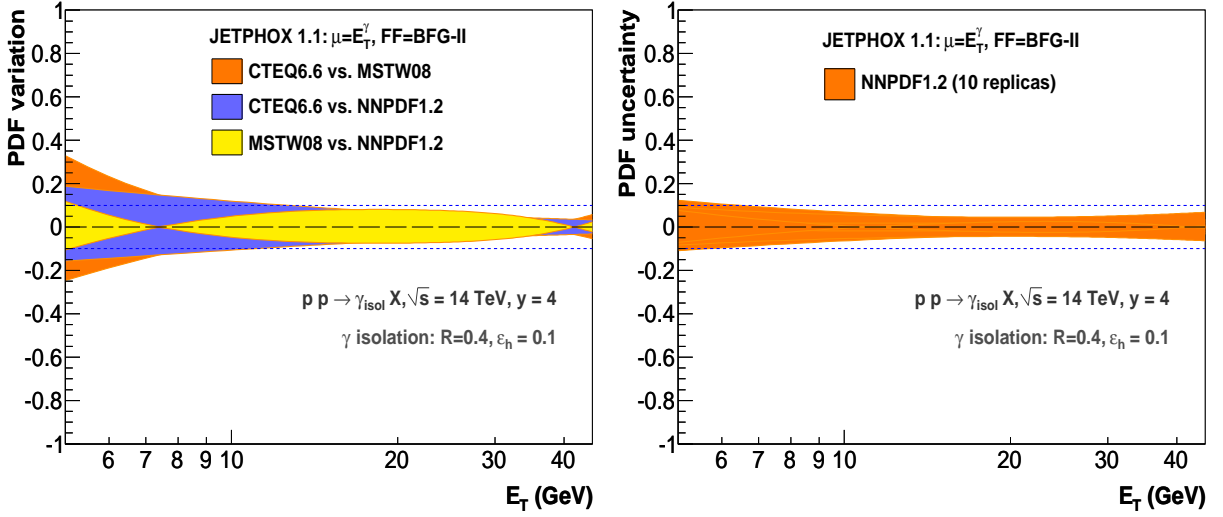


FIG. 9: Fractional differences between the isolated photon spectrum in  $p$ - $p$  collisions at  $\sqrt{s} = 14$  TeV at *forward* rapidities ( $y = 4$ ) obtained with JETPHOX (scales fixed at  $\mu = E_T^\gamma$ , FF set to BFG-II) using: (a) three different PDF parametrizations (CTEQ6.6, MSTW08 and NNPDF1.2), and (b) ten NNPDF1.2 replicas over the reference parametrization of the same PDF set. The dashed lines indicate a  $\pm 10\%$  uncertainty.

rapidities.

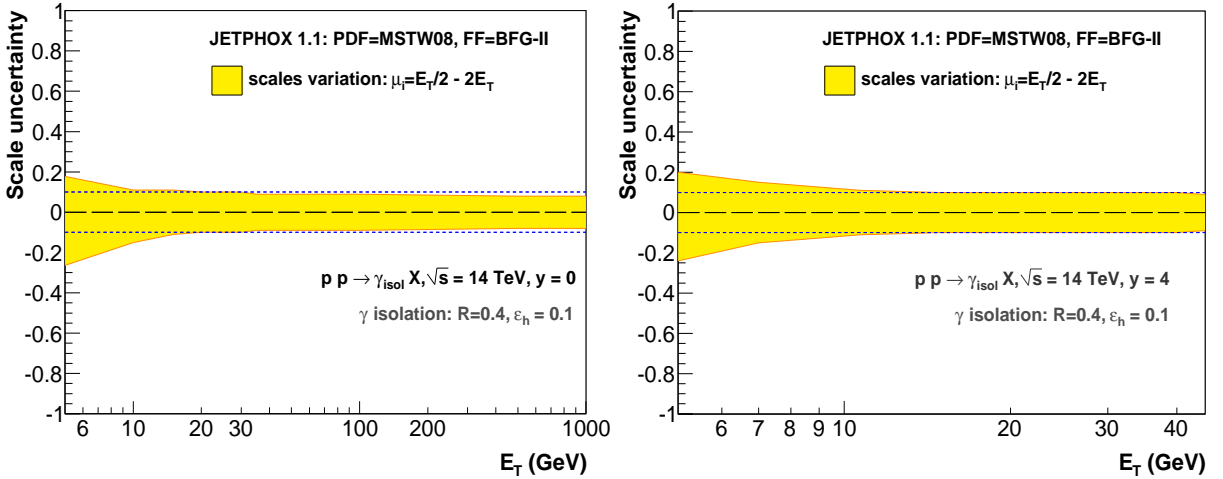


FIG. 10: Scale uncertainty plotted as the fractional differences between the isolated photon  $E_T$ -differential cross section in  $p$ - $p$  at  $\sqrt{s} = 14$  TeV at central ( $y = 0$ , left plot) and forward ( $y = 4$ , right plot) rapidities with scales  $\mu = E_T^\gamma$  compared to that with scales:  $\mu = 0.5E_T^\gamma, 2E_T^\gamma$ . The dashed lines indicate a  $\pm 10\%$  uncertainty.

As aforementioned, global PDF fits do not reliably determine the gluon for  $x \lesssim 10^{-2}$  at low, yet perturbative,  $Q^2 \lesssim 20$  GeV<sup>2</sup> scales [42]. This is due partly to the lack of precise structure function data for  $x < 10^{-4}$  and mainly due to the fact that the copious DIS  $F_2$  results probe the quark distribution, while the gluon density is constrained by the evolution,  $\log(Q^2)$  dependence, of these data. In the low  $x$  region the available  $Q^2$  range decreases since  $x$  and  $Q^2$  are correlated ( $x \propto Q^2/s$ ) and the accuracy of the gluon determination becomes worse. The main motivation to use the LHC isolated photon spectra to help constrain the low- $x$  gluon density in the proton is summarized in the left plots of Figs. 8 and 9. Different PDFs predict isolated photon yields which, at the lowest  $E_T^\gamma$  values, differ by up to  $\pm 30\%$ . Most

of such differences arise from the different small- $x$  gluon densities implemented in the three PDF sets. Indeed, as seen in Fig. 3, the Compton quark-gluon scattering clearly dominates isolated  $\gamma$  production at the LHC and, as indicated by Fig. 1, the LHC data at forward (central) rapidities probes parton fractional momenta around  $x = 10^{-4}$  (resp.  $x = 10^{-2}$ ). It is not unexpected that the largest PDF-dependent variations of the yields are observed in the low  $E_T^\gamma$  range since it is indeed at moderate virtualities that the gluon density is more uncertain. The minimum photon  $E_T \approx 5$  GeV considered here is pretty optimistic from an experimental point-of-view – the reconstruction and isolation of photons becomes more challenging with decreasing transverse energies – but it still corresponds to relatively large scales of order  $Q^2 \approx 25$  GeV<sup>2</sup>. Having the possibility to measure isolated photons with lower, but still perturbative, momenta around  $E_T^\gamma \approx 3$  GeV would provide even more stringent constraints on the low- $x$  gluon distributions.

One can take full advantage of the measured isolated photon results to better determine  $g(x, Q^2)$ , by including them in future global-fit analyses. Indeed, as seen in Fig. 10, the scale uncertainties at low  $E_T^\gamma$  are relatively large ( $\pm 20\%$ ) and thus a simple direct spectral comparison of the experimental  $E_T^\gamma$ -differential cross sections to the theoretical predictions will not unambiguously indicate the preferred PDF parametrization. The latest works of the NNPDF collaboration [27] use, for example, about 3500 experimental points to carry out their PDF fits, including DIS ( $F_2$ ,  $F_L$  and  $F_2^{\text{charm}}$ ) and proton-(anti)proton (Drell-Yan, vector-boson and jets) results. Yet, in the small- $x$  region the available experimental statistics is quite limited: just about 19 (126) data-points below  $x = 10^{-4}$  (resp.  $x = 10^{-3}$ ), among which only  $F_L$  is directly sensitive to the gluon. In these regions where there are little or no experimental constraints on the gluon, the most important source of the PDF uncertainty is due to the parametrization bias. Inclusion of new data-sets is basic to improve the central value of the PDFs and reduce their associated uncertainties. In that respect, including 10 – 20 data-points from forward isolated photon spectra at  $\sqrt{s} = 14$  TeV, will place new direct experimental constraints on the gluon distribution at  $x = 10^{-4}$ . The effect of these data on future PDF parametrizations might be larger if the existing measurements have inconsistencies which previously have not been accounted for. All in all, this work indicates that the combined photon data at all energies – about 350 data-points collected so far plus  $\mathcal{O}(100)$  new data-points expected from the four experiments at the LHC – provide new useful constraints of the gluon distribution in a wide  $(x, Q^2)$  range.

## V. CONCLUSIONS

We have compared the most recent measurements of isolated photon spectra in  $p\bar{p}$  collisions at  $\sqrt{s} = 1.96$  TeV [18, 20] with next-to-leading-order calculations with updated parton distributions functions (PDFs) in the proton. Previous data-theory comparisons [16, 18, 20] used relatively older PDF sets. The  $E_T$ -differential spectra at Tevatron can be equally well reproduced by the CTEQ6.6, MSTW08 and NNPDF1.2 global fit parametrizations within the existing experimental and theoretical uncertainties. Differences in the isolated photon cross sections for different PDF sets are in the range 5% – 10%, with the MSTW08 spectrum being somewhat in between the spectra computed with the two other PDFs. Theoretical uncertainties linked to the scales choices  $\mu_i = E_T^\gamma/2 - 2E_T^\gamma$  result in around  $\pm 10\%$   $E_T^\gamma$ -independent changes in the NLO cross sections. The choice of parton-to-photon fragmentation function (FF) does not introduce any additional theoretical uncertainty as the isolation criteria help to keep the contribution of fragmentation photons to the total prompt photon yield well below the fifteen percent at all transverse energies, and differences between FFs are a few percent of this remaining 15% contribution.

We have also presented the NLO isolated photon spectra expected in  $p\bar{p}$  collisions at the top LHC energy for central ( $y = 0$ ) and forward ( $y = 4$ ) rapidities and determined the associated theoretical uncertainties. At  $\sqrt{s} = 14$  TeV, the prompt photon cross sections (above 10 GeV) are more than a factor of seven larger than at Tevatron, and the parton fractional momenta probed are relatively small, down to  $x \approx 10^{-3}$  (resp.  $10^{-5}$ ) at mid (resp. forward) rapidity. Since the quark-gluon Compton process is found to represent about two thirds of the total isolated photon cross section at the LHC for standard isolation cuts, such a measurement promises to provide an interesting direct measurement to the relatively unconstrained low- $x$  gluon density  $g(x, Q^2)$  in the proton. The three PDFs studied yield central values of the photon spectrum which differ at most by  $\pm 15\%$  at  $y = 0$  and by  $\pm 30\%$  at  $y = 4$  in the low- $E_T^\gamma$  region of the spectra, whereas the experimental (associated with the calibration of the energy scale in the electromagnetic calorimeters) and the theoretical (linked to the choice of the renormalisation, factorisation,

and fragmentation scales) uncertainties are of  $\mathcal{O}(10 - 20\%)$ . To finalize, we have presented arguments to motivate the inclusion of the LHC photon data in future PDF global-fit analyses.

In summary, given (i) the high-quality isolated photon measurements available or expected at collider energies, (ii) the good agreement between the existing RHIC and Tevatron (except for the lowest  $E_T^\gamma$  bins) data and NLO calculations, and (iii) the large statistics photon data expected to be collected at various rapidities at the LHC, it is worth to reconsider the inclusion of the combined photon collider data measured in proton-(anti)proton collisions – about 350 data-points collected so far plus  $\mathcal{O}(100)$  new data-points expected from the four experiments at the LHC – in global-fit PDF analyses. Such data provide direct extra constraints on the gluon PDF in a wide  $(x, Q^2)$  range.

### Acknowledgments

We are grateful to François Arleo for many discussions and a careful reading of previous versions of this manuscript, as well as to Joan Rojo for valuable feedback on the NNPDF parton distributions and for useful comments on the document. Discussions with Thierry Gousset are also acknowledged. DdE is partially supported by the 7th EU Framework Programme (contract FP7-ERG-2008-235071).

- 
- [1] J. F. Owens, *Rev. Mod. Phys.* **59** (1987) 465.
  - [2] T. Binoth, J. P. Guillet, E. Pilon and M. Werlen, *Eur. Phys. J. direct C* **4** (2002) 7.
  - [3] P. Aurenche, A. Douiri, R. Baier, M. Fontannaz and D. Schiff, *Phys. Lett. B* **140** (1984) 87; P. Aurenche, R. Baier, M. Fontannaz and D. Schiff, *Nucl. Phys. B* **297** (1988) 661.
  - [4] L.E. Gordon and W. Vogelsang, *Phys. Rev. D* **50** (1994) 1901.
  - [5] A. V. Lipatov and N. P. Zotov, *J. Phys. G* **34** (2007) 219; S. P. Baranov, A. V. Lipatov and N. P. Zotov, *Phys. Rev. D* **77** (2008) 074024.
  - [6] M. V. T. Machado and C. B. Mariotto, *Eur. Phys. J. C* **61** (2009) 871.
  - [7] B. Z. Kopeliovich, E. Levin, A. H. Rezaeian and I. Schmidt, *Phys. Lett. B* **675** (2009) 190.
  - [8] E. Laenen, G. Oderda and G. Sterman, *Phys. Lett. B* **438** (1998) 173; S. Catani, M. L. Mangano and P. Nason, *JHEP* **9807** (1998) 024; D. de Florian and W. Vogelsang, *Phys. Rev. D* **72** (2005) 014014; T. Becher and M. D. Schwartz, *JHEP* **1002** (2010) 040.
  - [9] P. Aurenche, R. Baier, M. Fontannaz, J. F. Owens and M. Werlen, *Phys. Rev. D* **39** (1989) 3275.
  - [10] W. Vogelsang and A. Vogt, *Nucl. Phys. B* **453** (1995) 334.
  - [11] L. Bourhis, M. Fontannaz and J. P. Guillet, *Eur. Phys. J. C* **2** (1998) 529.
  - [12] Z. Belghobsi, M. Fontannaz, J. P. Guillet, G. Heinrich, E. Pilon and M. Werlen, *Phys. Rev. D* **79** (2009) 114024.
  - [13] F. Aversa, P. Chiappetta, M. Greco and J.Ph. Guillet, *Nuc. Phys. B* **327** (1989) 105; P. Aurenche, P. Chiappetta, M. Fontannaz, J.Ph. Guillet and E. Pilon, *Nuc. Phys. B* 399 (1993) 34.
  - [14] M. Klein and R. Yoshida, *Prog. Part. Nucl. Phys.* **61** (2008) 343.
  - [15] W. Vogelsang and M. R. Whalley, *J. Phys. G* **23** (1997) A1.
  - [16] P. Aurenche, M. Fontannaz, J. P. Guillet, E. Pilon and M. Werlen, *Phys. Rev. D* **73** (2006) 094007.
  - [17] S. S. Adler *et al.* [PHENIX Collaboration], *Phys. Rev. D* **71** (2005) 071102; S. S. Adler *et al.* [PHENIX Collaboration], *Phys. Rev. Lett.* **98** (2007) 012002.
  - [18] T. Aaltonen *et al.* [CDF Collaboration], *Phys. Rev. D* **80** (2009) 111106.
  - [19] L. Apanasevich *et al.* [E706 collaboration], *Phys. Rev. Lett.* **81** (1998) 2642; *Phys. Rev. D* **70** (2004) 092009.
  - [20] V. M. Abazov *et al.* [D0 Collaboration], *Phys. Lett. B* **639** (2006) 151 [Erratum-ibid. B **658** (2008) 285].
  - [21] A. D. Martin, R. G. Roberts, W. J. Stirling and R. S. Thorne, *Eur. Phys. J. C* **14** (2000) 133.
  - [22] J. Pumplin *et al.* [CTEQ Collaboration], *J. High Energy Phys.* **0207** (2002) 012.
  - [23] A. D. Martin, R. G. Roberts, W. J. Stirling and R. S. Thorne, *Phys. Lett. B* **604** (2004) 61.
  - [24] P. M. Nadolsky *et al.*, *Phys. Rev. D* **78** (2008) 013004.
  - [25] A. D. Martin, W. J. Stirling, R. S. Thorne and G. Watt, *Eur. Phys. J. C* **63** (2009) 189; A. D. Martin, W. J. Stirling, R. S. Thorne and G. Watt, *Eur. Phys. J. C* **14**, 133 (2000).
  - [26] R. D. Ball *et al.* [NNPDF Collaboration], *Nucl. Phys. B* **809**, 1 (2009) [Erratum-ibid. B **816** (2009) 293]; R. D. Ball *et al.* [The NNPDF Collaboration], *Nucl. Phys. B* **823** (2009) 195.
  - [27] R. D. Ball, L. Del Debbio, S. Forte, A. Guffanti, J. I. Latorre, J. Rojo and M. Ubiali, *Nucl. Phys. B* 838 (2010) 136.
  - [28] B. Alessandro *et al.* [ALICE Collaboration], *J. Phys. G: Nucl. Part. Phys.* **32** (2006) 1295.
  - [29] G. Aad *et al.* [ATLAS Collaboration], arXiv:0901.0512.
  - [30] A. de Roeck (ed.) [CMS Collab.], *J. Phys. G* **34** (2007) 995.
  - [31] LHCb Reoptimized Detector Design and Performance TDR, CERN/LHCC 2003-030, LHCb TDR 9.
  - [32] P. Aurenche, T. Binoth, M. Fontannaz, J.-P. Guillet, G. Heinrich, E. Pilon and M. Werlen, [http://lapweb.in2p3.fr/lapth/PHOX\\_FAMILY/jetphox.html](http://lapweb.in2p3.fr/lapth/PHOX_FAMILY/jetphox.html)
  - [33] J. H. Kuhn, A. Kulesza, S. Pozzorini and M. Schulze, *JHEP* **0603** (2006) 059.
  - [34] S. Catani, M. Fontannaz, J.-P. Guillet and E. Pilon, *JHEP* **0205** (2002) 028.
  - [35] See e.g. *Proceeds. MPI'08 Workshop*, Perugia, 2008; DESY-PROC-2009-06; arXiv:1003.4220.
  - [36] M. R. Whalley, D. Bourilkov and R. Group, arXiv:hep-ph/0508110; <http://hepforge.cedar.ac.uk/lhapdf/>
  - [37] T. Sjostrand, S. Mrenna and P. Skands, *JHEP* **0605** (2006) 026.
  - [38] R. Ichou and D. d'Enterria, in preparation.
  - [39] G. Diana, J. Rojo and R.-D. Ball, arXiv:1006.4250.
  - [40] M. Gluck, E. Reya and A. Vogt, *Phys. Rev. D* **48** (1993) 116 [Erratum-ibid. D **51** (1995) 1427].

- [41] D. Buskulic *et al.* [ALEPH Collaboration], Z. Phys. C **69** (1996) 365; K. Ackerstaff *et al.* [OPAL Collaboration], Eur. Phys. J. C **2** (1998) 39.
- [42] A. D. Martin, C. Nockles, M. G. Ryskin and T. Teubner, Phys. Lett. B **662** (2008) 252.